Highly Dispersed Ag₂SO₄ Nanoparticles Deposited on ZnO Nanoflakes as Photocatalysts

Wenrong Cao · Lifang Chen · Zhiwen Qi

Abstract Highly dispersed silver sulfate nanoparticles deposited on ZnO nanoflakes (ASZ) were successfully prepared by a simple solvothermal method with different silver contents. The prepared 3ASZ composite shows improved photocatalytic activity for rhodamine B degradation under UV–vis light irradiation compared with pure ZnO, Ag_2SO_4, and commercial TiO_2 (P25). The remarkable photocatalytic activity for ASZ composite maybe due to the synergistic effects between photo-reduced Ag and SO_4^{2-} on the surface of ZnO nanoflakes, which promote efficient separation of electron–hole pairs.

1 Introduction

In recent years, great efforts have been focused on designing and fabricating novel semiconductor photocatalysts with suitable band gap for solving energy shortages and environmental pollution [1–3]. In comparison with conventional technologies, semiconductor photocatalysts can directly utilize UV even solar light to eliminate water contaminants, especially azo dyes, without generating any harmful by-products, which can be considered as a promising approach in a variety of environmental processes [4, 5]. ZnO, a n-type semiconductor with a similar band gap

(3.37 eV) to TiO_2, has been widely applied in electronics, optics, sensors and catalysts. For these applications, it is preferred to control the morphologies of ZnO. In the past several years, a variety of ZnO morphologies, such as nanorods, dandelions, hollow spheres, hexagonal rings, have been constructed. Among morphology-dependent properties, the shape control of ZnO is indispensable to satisfy the unique applications. In addition, ZnO as one of traditional photocatalysts for degradation of organic dyes has drawn a special attention for a long time owing to its suitable band gap, lower cost, non-toxicity, and regulatable morphologies [6, 7]. It is reported that the competition between rapid recombination and efficient segregation of photogenerated charge carriers plays a very important role on photocatalytic performance of semiconductors [8, 9]. However, the electron–hole pairs generated from ZnO-based photocatalysts display fast recombination rate, which limits the quantum efficiency of ZnO and strongly impedes the enhancement of photocatalytic activity [10, 11]. Therefore, the synthesis of novel ZnO-based nanostructures in combination with its excellent performance is meaningful and challenging.

Many methods have been employed to improve photocatalytic property of semiconductors, including purposive nonmetal, metal, or noble metal doping, and recombining with other semiconductors [12, 13]. It is widely acceptable that the couple of different semiconductors with suitable band potential, such as V_2O_5/ZnO, $BiVO_4$/CeO_2, etc., can act as one of the most efficient pathways. Compared with single semiconductor, the coupled composite can absorb wide ranges of spectral energy, dominate the excited electrons injected from one semiconductor into the other, which can speed up separation rate of photoinduced charge carriers, and consequently enhance photocatalytic performance [14, 15]. Accordingly, it is highly advantageous to

W. Cao · L. Chen (✉) · Z. Qi (✉)
State Key Laboratory of Chemical Engineering, East China University of Science and Technology, Shanghai 200237, China
e-mail: lchen@ecust.edu.cn

Z. Qi
e-mail: zwqi@ecust.edu.cn

improve photocatalytic activity by developing novel coupled composite photocatalysts. Silver-based nanoparticles as promising doping candidates deposited on some wide band gap semiconductors (TiO_2, BiOBr, etc.) have aroused a great interest recently owing to its accelerating migration and separation of photoexcited carriers through good interfacial adhesion between the two semiconductors [16, 17]. Cheng et al. have prepared a novel Ag/AgBr/BiOBr hybrid, which exhibits very high visible-light-induced photocatalytic activity because of the excellent transfer of photogenerated electrons and holes [18]. Zhang et al. have fabricated Ag_3PO_4/SnO_2 composite with superior high photocatalytic activity and good thermal stability [19]. Silver sulfate, a non-alkali metal sulfate, is utilized in electrochemical devices such as solid state batteries and SO_x gas sensors owing to its high cationic conductivity, and catalyst for the determination of chemical oxygen demand. Although different silver-based semiconductors have been employed as photocatalysts, Ag_2SO_4-based photocatalysts have not been reported so far. Therefore, it is a challenge to prepare stable and high activity of Ag_2SO_4-based composite photocatalysts.

Herein, we report highly dispersed Ag_2SO_4 nanoparticles (NPs) deposited on the surface of ZnO nanoflakes by a simple solvothermal method. The synthesized Ag_2SO_4/ZnO photocatalysts are found to display higher photocatalytic performance than pure ZnO and Ag_2SO_4 for rhodamine B (RhB) photodegradation under UV–visible light irradiation. In addition, the mechanism of enhanced photocatalytic activity is systematically investigated. It is found that the synergistic effects between photo-reduced Ag NPs and SO_4^{2-} are considered as the key factors for the enhanced photocatalytic activity of the double semiconductors.

2 Experimental Details

2.1 Materials

Commercial TiO_2 (P25) was purchased from Degussa. $Zn(CH_3COO)_2 \cdot 2H_2O$, thiourea, $AgNO_3$, Na_2SO_4, poly (vinyl pyrrolidone) (PVP, Mw = 30,000), ethylene glycol (EG) and Rhodamine B (RhB) were supplied by Aladdin Inc. and used without further purification.

2.2 Synthesis of Ag₂SO₄ Nanoparticles Deposited on ZnO Nanoflakes

In a typical process, 0.33 g of $Zn(CH_3COO)_2 \cdot 2H_2O$, 0.23 g of thiourea and 1.2 g of PVP were dissolved in 32 ml of EG with constant stirring to yield transparent solution, followed by dropwise addition of 100, 300, or 500 μl of $AgNO_3$ solution (1 M in deionized water). The transparent solution immediately turned into black suspensions. The above suspensions were placed into a Teflon-lined stainless steel autoclave, maintained at 150 °C for 3 h, and then naturally cooled to room temperature. The precipitates were separated by centrifugation, washed with deionized water and ethanol for several times, and dried at 60 °C for 6 h. The obtained powder was subsequently calcined at 500 °C for 4 h and 700 °C for 4 h. Thus, the high quality Ag_2SO_4/ZnO composites were fabricated and named as 1ASZ, 3ASZ, 5ASZ, respectively. For comparison, pure ZnO or Ag–ZnO photocatalyst was prepared by similar procedures without $AgNO_3$ solution or thiourea, respectively.

2.3 Characterization

The crystalline phase of the prepared samples was determined by powder X-ray diffraction analysis (XRD; Rigaku D/MAX-2550 diffractometer) with Cu-Kα radiation ($\lambda = 1.5406$ Å) in the range of $2\theta = 20°–70°$ at room temperature. The X-ray photoelectron spectroscopy (XPS) measurements were performed by a Multilab 2000 XPS system with a monochromatic Mg Kα source and a charge neutralizer. All of the binding energies were referenced to the C 1s peak at 284.6 eV of the surface adventitious carbon. The surface morphologies and microstructures of the products were observed by a field-emission electron scanning microscope (FE-FEM, Hitachi S-4800) and high-resolution transmission electron microscopy (HR-TEM, JEM-2100). The UV–vis diffuse reflectance spectra (DRS) were obtained by PerkinElmer Lamda 35 UV–vis spectrometer in a wavelength range of 200–800 nm, using $BaSO_4$ as a reference.

2.4 Photocatalytic Activity Test

The photocatalytic activity of photocatalysts was tested by degradation of RhB solution using a 350 W xenon lamp under UV–vis light irradiation at room temperature. Typically, 30 mg of sample was added in RhB aqueous solution (30 mg/l, 30 ml) and pH was adjusted by nitric acid or sodium hydroxide. Then the suspension liquid was sonicated for 15 min, and magnetically stirred in dark for 2 h in order to establish adsorption–desorption equilibrium between photocatalysts and RhB molecules prior to light irradiation. During illumination, approximately 2.0 ml of suspensions including the sample powders and dyes were collected at the regular intervals from the reactor and centrifuged to remove the solid particles. The dye solutions were analyzed by recording the maximum absorption wavelength at 553 nm via a PerkinElmer Lamda 35 UV–vis spectrophotometer.

3 Results and Discussion

3.1 Catalyst Characterization

A number of analytical studies have been carried out to obtain information about Ag_2SO_4 nanoparticles deposited on ZnO nanoflakes (ASZ). The crystal structures of as-synthesized products are revealed by powder X-ray diffraction (XRD) in Fig. 1. The XRD pattern of 3ASZ sample without calcination can be identified as standard wurtzite ZnS (JCPDS card No. 36-1450) and weak Ag_2S peaks in Fig. 1a. The ZnS and Ag_2S crystal formation is due to the generated isothiourea, which is produced by the isomerization of thiourea during the synthesized process, with a strong nucleophilic substitution of the Zn^{2+} and Ag^+ in mixed salt solution [20]. Figure 1b–e shows the XRD patterns of the calcined samples, which are in good agreement with (101) (002) (101), and (110) planes of standard wurtzite ZnO (JCPDS card No. 36-1451). The sharp and narrow peaks in Fig. 1b indicate that neat ZnO has high crystallinity without any Ag_2SO_4 deposition during preparation. For Ag_2SO_4/ ZnO composites, besides wurtzite ZnO, the diffraction peaks indexed to orthorhombic Ag_2SO_4 (JCPDS card No. 27-1403 can also be observed in Fig. 1c–e. The disappearance of ZnS and Ag_2S diffraction peaks demonstrate that the as-synthesized samples can be completely converted to Ag_2SO_4/ZnO composite during high-temperature calcinations in the atmosphere. The intensity of the ZnO diffraction peaks is gradually decreased with increased Ag_2SO_4 contents. It is indicative of higher Ag_2SO_4 contents resulting in weaker ZnO diffraction peaks, which is owing to homogeneous distribution of doping Ag_2SO_4 nanoparticles [21]. In addition, in contrast to neat ZnO, Ag_2SO_4 deposited on ZnO nanoflakes have few peaks shift, which can be deduced that Ag_2SO_4 nanoparticles are only deposited on the surface of ZnO and do not destroy the lattice structure of ZnO [22].

In order to further investigate the chemical composition and chemical states of catalysts, the XPS analysis results were performed in Fig. 2. The binding energies of different elements were calibrated by C 1s at 284.6 eV. The peaks of Zn, O, Ag, S, and C elements have been detected for 3ASZ sample in the scan survey spectra. No other elements can be observed in the samples, as shown in Fig. 2a. C element might come from hydrocarbon contaminant from XPS instrument and carbon dioxide absorbed on the surface of the catalysts from air. It is confirmed that 3ASZ catalyst is composed of Zn, O, Ag, and S elements, which is consistent with previous XRD results. The high-resolution XPS spectra of the asymmetric O 1s for neat ZnO in Fig. 2b can make contributions to lattice oxygen species of ZnO at a lower binding energy 530.0 eV and chemisorbed oxygen of the surface hydroxyl (−OH) at a higher binding energy 531.8 eV [23], while the O 1s peak of 3ASZ shows three
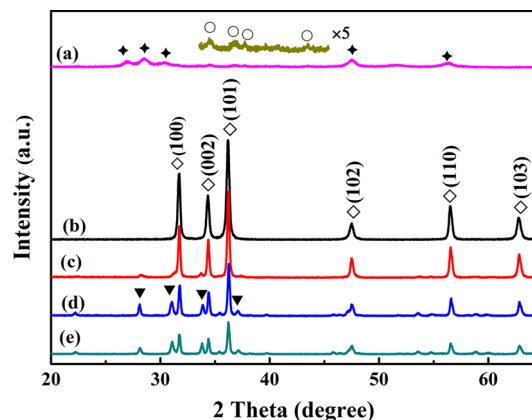

Fig. 1 XRD patterns of *a* as-synthesized 3ASZ photocatalyst without calcination, *b* neat ZnO, *c* 1ASZ, *d* 3ASZ and *e* 5ASZ after calcination (*Filled diamond* ZnS, *open circle* Ag_2S, *open diamond* ZnO, *filled inverted triangle* Ag_2SO_4)

kinds of oxygen species at 530.0, 531.3, 532.5 eV in Fig. 2c. In addition to above two kinds of oxygen state, the peak at 531.3 eV is attributed to the O species in sulphate [24]. Moreover, the oxygen binding energy of surface absorbed hydroxyl shifts slightly to higher value in comparison with that of neat ZnO due to the deposition of Ag_2SO_4 nanoparticles. In addition, it is reported that the standard binding energy for Ag $3d_{3/2}$ and Ag $3d_{5/2}$ of metal Ag^0 are about at 368.2 and 374.2 eV, whereas 367.4 and 373.9 eV are assigned to Ag^+ [25]. In our XPS spectra, the binding energy of Ag 3d peaks for 3ASZ at 367.1 and 373.1 eV are attributed to Ag^+. Moreover, the Ag $3d_{3/2}$ and Ag $3d_{5/2}$ peaks are not completely split, which can be only attributed to the Ag^+ of Ag_2SO_4 [26]. Previous studies show that S 2p binding energies for CuS, S^{4+}, and S^{6+} are at 162.0 [27], 167.5 [24], and 168.5 eV [28], respectively. The only peak at 168.4 eV corresponding to S 2p is observed in Fig. 2e and can belong to oxidized form of sulphur (SO_4^{2-} species).

The optical absorption properties of all samples were investigated by UV–vis diffuse reflectance spectroscopy (DRS). Figure 3a shows that all samples have strong absorption in ultraviolet range. In comparison with pure ZnO, the absorption edges of ASZ composites have slight red-shifts. The shift of absorption edge towards longer wavelengths depends on Ag_2SO_4 contents, which clearly indicates the decrease in the band gap energy of ZnO. The shift may be due to a partial interfacial charge transfer between ZnO and Ag_2SO_4. On the other hand, compared with neat ZnO and Ag_2SO_4, ASZ composites exhibit obvious absorption shoulders in the wavelength range of 425–520 nm. The visible-light-response enhancement of ASZ may stem from Ag_2SO_4 particles anchored on the surface of ZnO nanoflakes, which should have better photocatalytic activity than pure ZnO and Ag_2SO_4. The

Fig. 2 a The survey spectra of ZnO and 3ASZ, and the high-resolution XPS spectra of **b** O 1s peak for pure ZnO, **c** O 1s peak for 3ASZ, **d** Ag 3d peak and **e** S 2p peak for 3ASZ
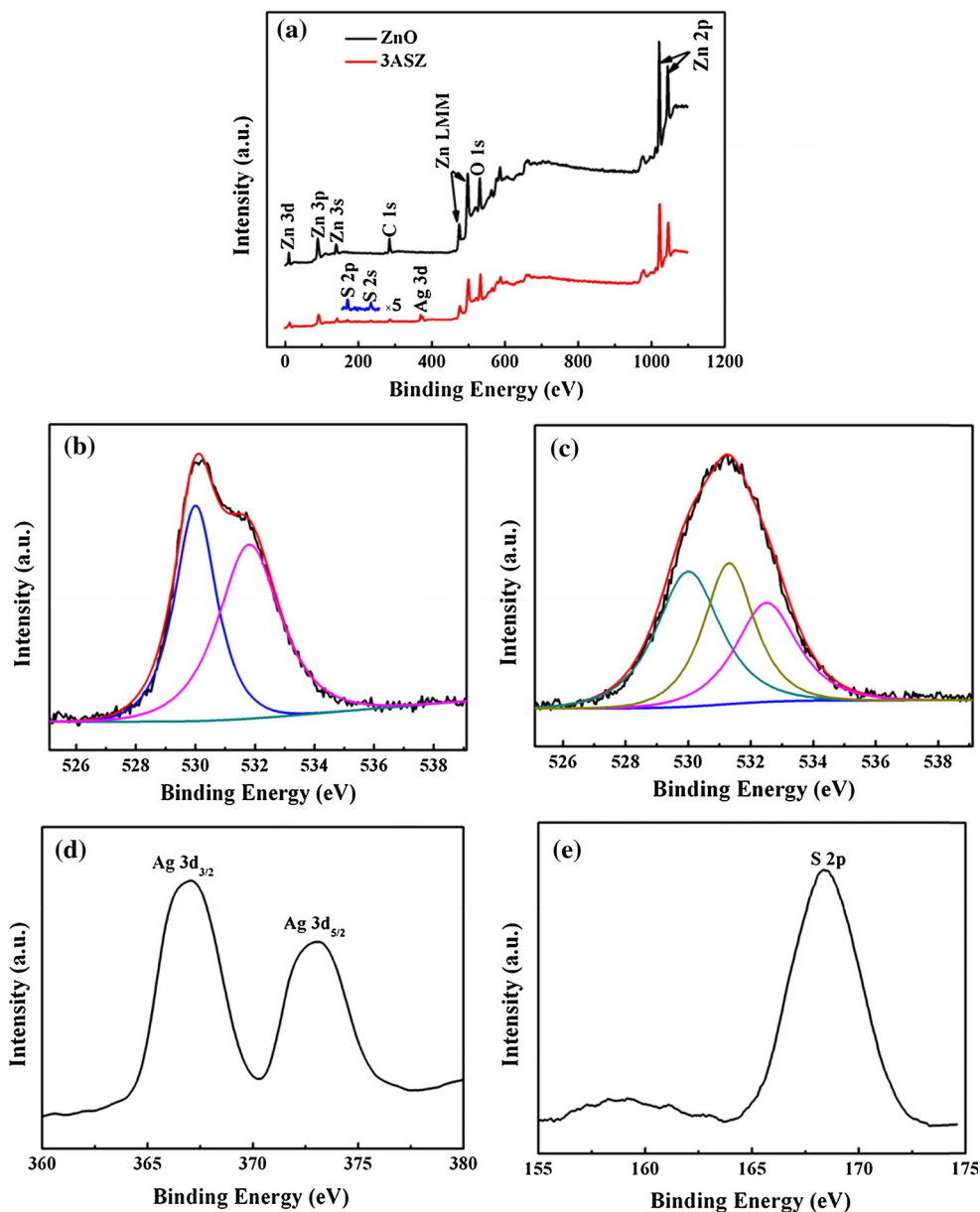

direct bandgap energies of pure ZnO, 1ASZ, 3ASZ and 5ASZ are evaluated by Kubelka–Munk function [29].

$$\alpha h\nu = A(h\nu - E_g)^{n/2} \tag{1}$$

where α, ν, A and E_g are the absorption coefficient, light frequency, absorption constants, and band gap, respectively. Among them, n is 1 for direct interband transition and 4 is for indirect interband transition. Here ZnO is a direct band gap semiconductor, and the value of n equals 1. Thus the band gap energy can be estimated to be the $h\nu$-axis intercept of linear portion in Fig. 3b. The direct bandgap energies for pure ZnO, 1ASZ, 3ASZ and 5ASZ are 3.11, 3.07, 3.04 and 3.05 eV, respectively. It can be clearly observed that there are narrowed bandgaps for ASZ composites.

The detailed morphology and microscopic structure of 3ASZ were presented in Fig. 4. The FESEM analysis shows that 3ASZ is composed of uniform nanoflakes with edge thicknesses of about 10–20 nm and smooth surface in Fig. 4a. The representative TEM images of 3ASZ are clearly shown in Fig. 4b, and demonstrate that Ag₂SO₄ nanoparticles with average sizes about 3–8 nm are highly dispersed on the surfaces of the ZnO nanoflakes. The high-resolution TEM image, obtained from the edge of the selected TEM image as shown in Fig. 4c, clearly shows two different kinds of the lattice fringes. The lattice fringes of 3ASZ are 0.28 and 0.26 nm that correspond to the distance of ZnO (100) and Ag₂SO₄ (022) planes, respectively. The continuous lattice spacing between Ag₂SO₄ and ZnO indicates the surface-junction of Ag₂SO₄–ZnO, which
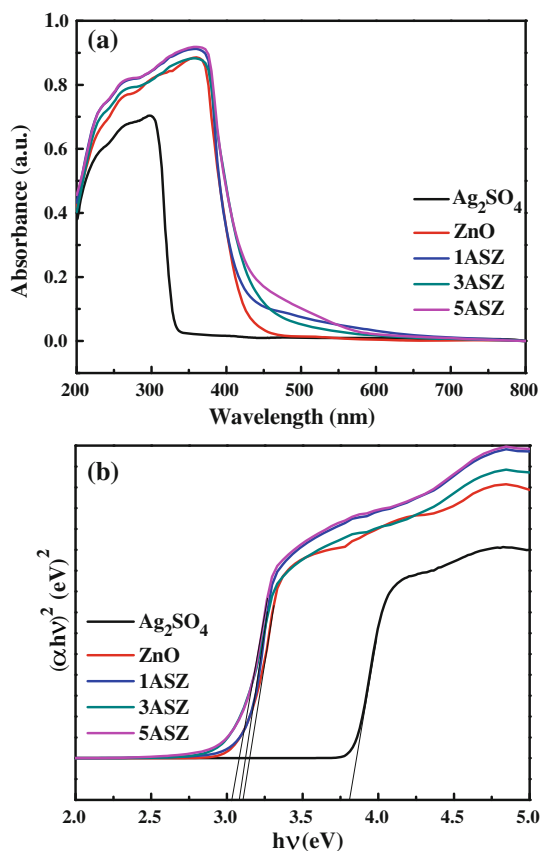
Fig. 3 a UV–vis diffuse reflectance spectra and **b** plots of $(\alpha h\nu)^2$ vs hv for Ag_2SO_4, ZnO, 1ASZ, 3ASZ and 5ASZ

could be expected to accelerate charge migration and facilitate photogenerated electron transfer during photocatalytic reaction.

3.2 Photocatalytic Activity

Nanostructured semiconductor composites can act as efficient photocatalysts to improve separation efficiencies of electron–hole pairs and extend energy ranges of photoexcitation, and thus exhibit superior photocatalytic activity [30, 31]. The photocatalytic property of Ag_2SO_4 nanoparticles deposited on ZnO nanoflakes was examined by RhB degradation under UV–vis light irradiation at room temperature. The typical time-dependent absorption spectra of RhB solution in the presence of 3ASZ are shown in Fig. 5a. The intensity of absorption peaks at 553 nm decreases dramatically with increased irradiation time, suggesting that RhB degradation is occurring. The reaction is finished within only 6 min, indicating that Ag_2SO_4/ZnO composites can efficiently catalyze RhB degradation. Figure 5b exhibits photocatalytic degradation curves of RhB with different photocatalysts, where C_0 and C are initial RhB concentration after equilibrium concentration and residue concentration of RhB after time interval irradiation, respectively. In the

absence of photocatalyst, RhB solution remains unaltered under longtime UV–vis light irradiation, showing the structure of RhB is very stable and the degradation can not occur. Under identical experimental conditions, the photocatalytic activities of Ag_2SO_4 particles, neat ZnO, and commercial P25 (TiO_2) were also performed. The RhB solution is completely degraded over P25 in 12 min, neat ZnO in 18 min, and Ag_2SO_4 particles in even longer time, as shown in Fig. 5b. 3ASZ composite can completely degrade RhB solution in only 6 min, and possess the most excellent photocatalytic performance in comparison with Ag_2SO_4 particles, ZnO, and P25. The photocatalytic degradation of organic dyes by metal oxide semiconductors can be described in terms of Langmuir–Hinshelwood model [32, 33]. As can be seen in Fig. 5c, the corresponding $\ln(C/C_0)$ versus irradiation time plots show good linearities, indicating that the photodegradation of RhB solution over different catalysts follows first-order kinetics. For 3ASZ sample, the reaction rate constant k reaches the maximum value of $0.63 \ min^{-1}$, which is 21.6, 2.5 and 2.4 times higher than those of pure Ag_2SO_4, ZnO and P25, respectively. The results indicate that the enhanced photocatalytic behaviour of the coupled photocatalysts denotes a synergetic effect between both semiconductors.

Additionally, the effect of the Ag_2SO_4 contents on the photodegradation efficiency was also investigated in Fig. 6a. Whatever, with decreased and increased amounts of Ag_2SO_4 nanoparticles, the photodegradation efficiency of 1ASZ and 5ASZ is lower than that of 3ASZ. But they have better photodegradation efficiency than that of neat ZnO. Therefore, the content of Ag_2SO_4 can greatly influence photocatalytic performance of Ag_2SO_4/ZnO composites. The reason maybe due to that Ag_2SO_4 deposited on the surface of ZnO nanoflakes can act as electron sinks attracting photogenerated electrons from ZnO. By contrast, photoinduced holes remain on the surface of ZnO, which can improve separation of the electron and hole pairs. However, if the amounts of Ag_2SO_4 particles is less or more than the optimized value, some Ag_2SO_4 nanoparticles may be insufficient or tend to aggregate, and could play a role of electron–hole recombination center to reduce the photocatalytic activity [34].

In wastewater treatment, adsorption and degradation of photocatalysts are importantly influenced by different pH in photocatalysis [35]. Therefore, the initial pH of dye solution has potential effects on photocatalytic activity of photocatalysts. Figure 6b exhibits reaction rate constant k on 3ASZ and P25 at different pH adjusted by nitric acid or sodium hydroxide, respectively. The removal efficiency of RhB over P25 maintains similar level in pH range from 4 to 9. It is interesting to note that 3ASZ remains better photocatalytic performance than that of P25 in all pH. Moreover, the highest rate of RhB degradation over 3ASZ is attained in
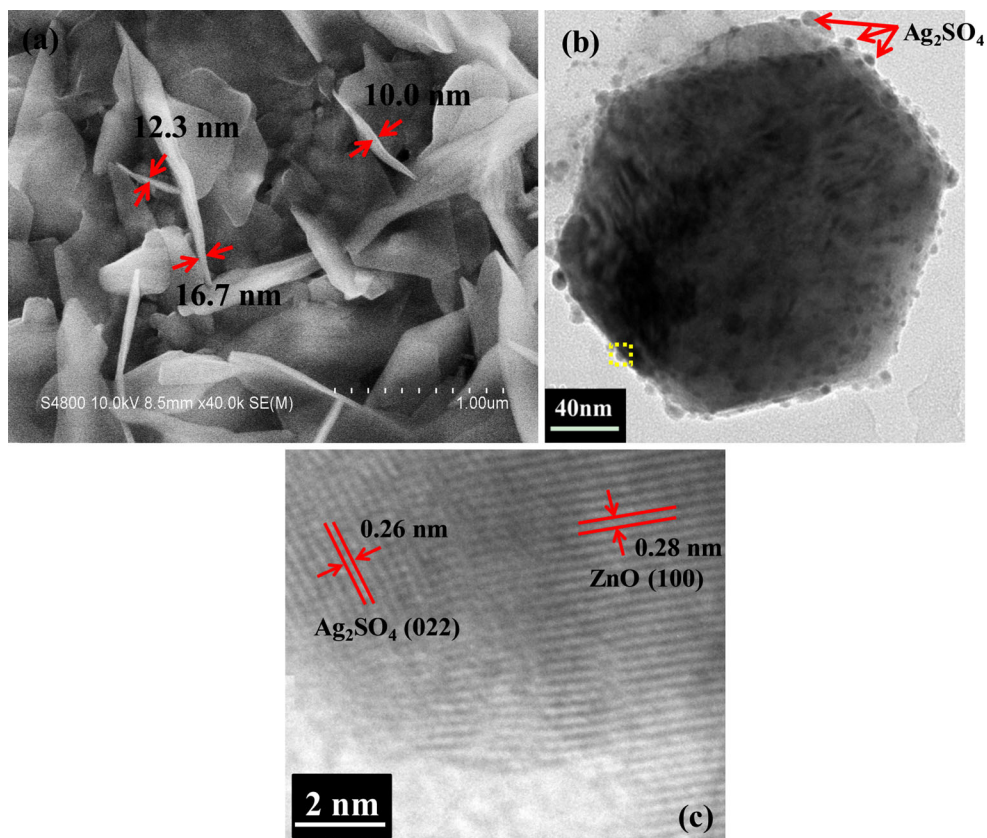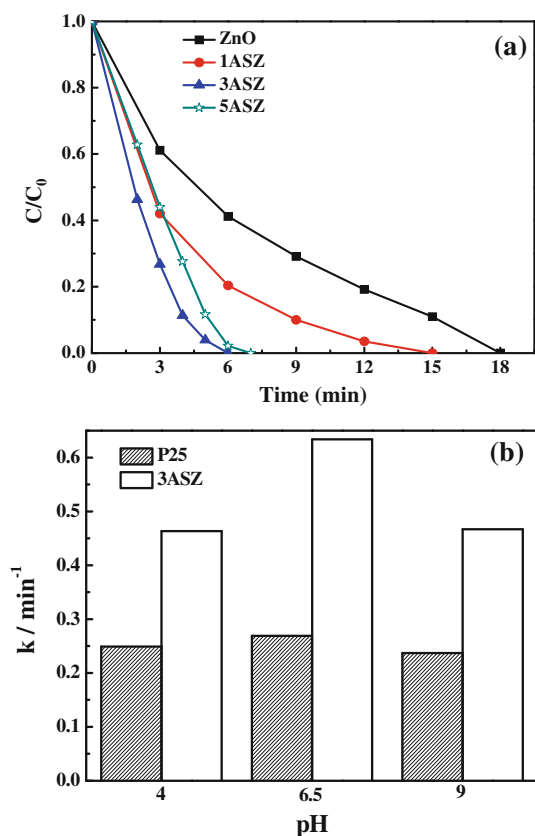
Fig. 4 **a** Typical FESEM image of 3ASZ, **b** TEM and **c** HRTEM images of 3ASZ
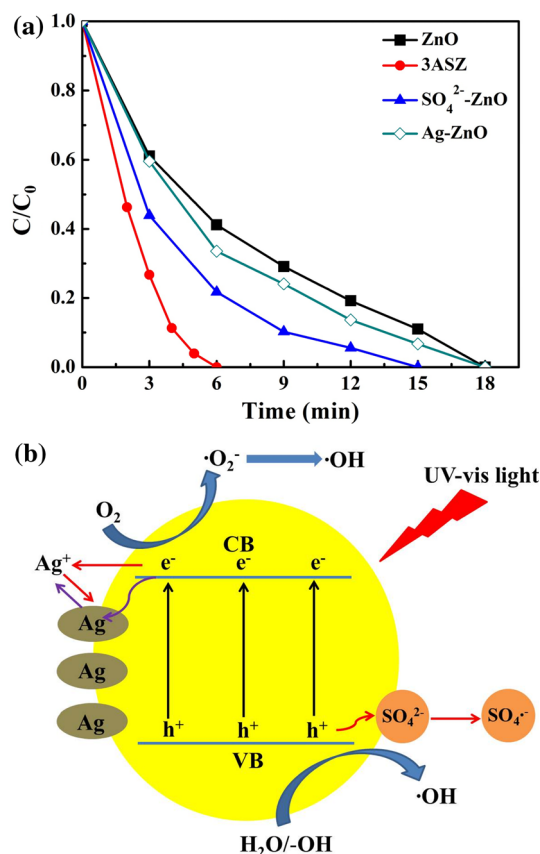
Fig. 5 **a** UV–vis absorbance spectra of RhB over 3ASZ, **b** photocatalytic efficiencies, and **c** the $\ln(C/C_0)$ versus time curves of RhB degradation over different photocatalysts (neat Ag₂SO₄ purchased from Aladdin Reagent)
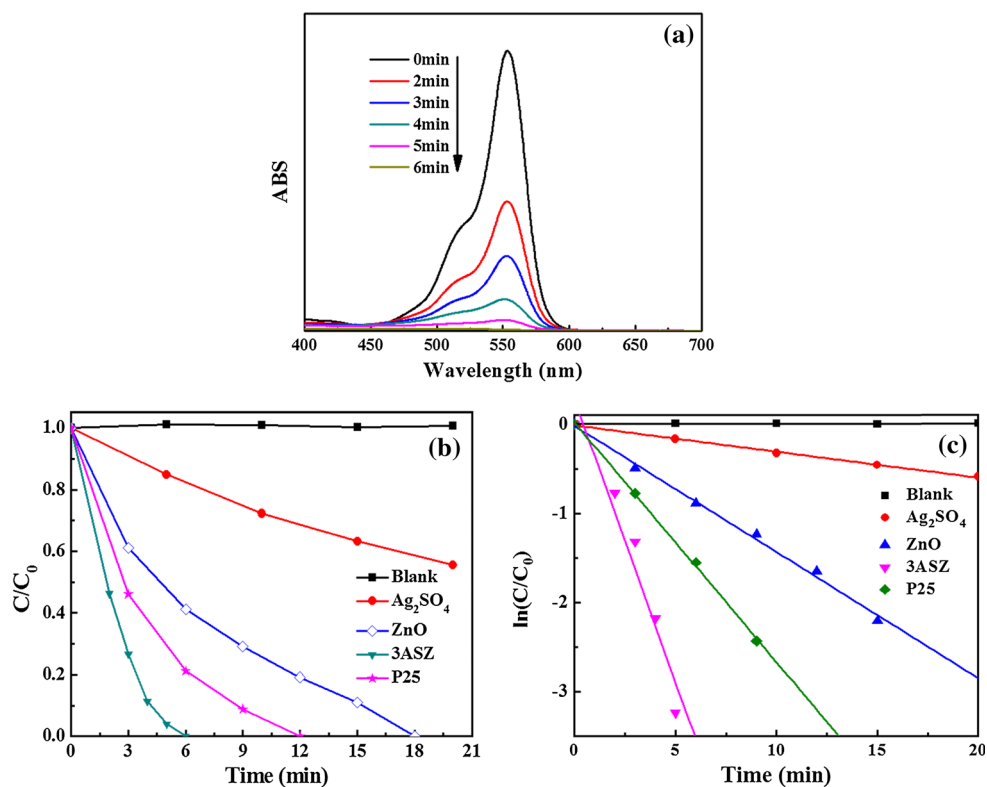
Fig. 6 a Comparison of photocatalytic activity over different ASZ samples on degradation of RhB and b pH effects of RhB solution on reaction rate constant k over P25 and 3ASZ

Fig. 7 a Controlled photocatalytic experiments of different catalysts and b schematic diagram of the electron–hole pairs separation over Ag_2SO_4/ZnO photocatalyst

neutral condition (pH 6.5). This indicates some important effects of pH on photocatalytic performance. To the best of knowledge in metal oxides, the adsorption of water molecules at superficial metal sites on the surface of metal oxides is dissociated and equivalent by metal hydroxyl groups (M–OH) due to their amphoteric behaviour. Both equilibrium media are positively charged $Zn–OH_2^+$ and negatively charged $Zn–O^-$. At low pH, the catalysts surface is positively charged, resulting in increasing electrostatic repulsion to RhB cations. As a result, the adsorption of RhB dye on the catalysts surface is dramatically reduced, and subsequently restrains the decomposition rate of RhB. Similar behaviour has been reported for photocatalytic efficiency of various semiconductors for azo-dyes degradation [35, 36]. At neutral or higher pH, surface is negatively charged by adsorbed large quantities of OH^-, which is a reaction medium for the decolorization process. The higher photocatalytic efficiencies in neutral or alkaline conditions are observed [35]. However, the removal efficiency over 3ASZ is reduced at pH 9 in this work. The decreased photocatalytic activity maybe attributed to the destroyed Ag_2SO_4 structure owing to slightly soluble Ag_2SO_4 reacted with OH^- in an alkaline environment [36].

3.3 Photocatalytic Mechanism

Ag_2SO_4/ZnO composite, especially 3ASZ, shows the prominent photocatalytic efficiency toward RhB solution degradation under UV–vis light irradiation. Therefore, it is important to investigate the relationship between the photocatalytic performance and surface properties of catalysts. However, the 3ASZ has low BET surface area of 1.38 m^2/g and pore volume of 0.004 cm^3/g, which could show negligible effects on photocatalytic performance. By contrast, the surface-junction, ultrathin nanoflakes and high crystallinity of as-synthesized Ag_2SO_4/ZnO photocatalyst can enhance charges diffusion to the surface of the catalysts, helping to accelerate the effective charges separation [37]. On the other hand, Ag_2SO_4/ZnO composite shows an obvious absorption shoulder in visible-light region compared with pure ZnO, leading to the enhanced efficiency of the photocatalytic reaction since more electron–hole pairs are generated under UV–vis light irradiation. Moreover, during the light irradiation process, Ag^+ in Ag_2SO_4 can accept photogenerated electrons and be gradually reduced into Ag NPs, which is a good electron acceptor. SO_4^{2-} as a strongly binding anion is anchored on the surface of ZnO,

thus affecting the photocatalytic activity [38]. The controlled photocatalytic experiments of Ag–ZnO and SO$_4^{2-}$–ZnO were performed in order to further confirm the positive effect of Ag$_2$SO$_4$ and explore the photocatalytic mechanism. The photocatalytic experiment of SO$_4^{2-}$–ZnO was performed by adding Na$_2$SO$_4$ and ZnO to RhB solution, as shown in Fig. 7a. The photocatalytic activity of Ag–ZnO and SO$_4^{2-}$–ZnO is slightly higher than that of neat ZnO, but obviously lower than that of 3ASZ. It demonstrates that the separate presence of Ag or SO$_4^{2-}$ cannot effectively improve the photocatalytic performance. Therefore, the enhanced photocatalytic activity of Ag$_2$SO$_4$/ZnO composite mainly results from the cooperative effect between photo-reduced Ag NPs and SO$_4^{2-}$. Previous studies have shown that the decomposition rate of dyes can be promoted by SO$_4^{2-}$ added as sodium salts, which may react with ·OH radical and h$^+$ and generate SO$_4^{·-}$, chemically shown in Eqs. (2) and (3) [38, 39]

$$SO_4^{2-} + h^+ \rightarrow SO_4^{·-} \tag{2}$$

$$SO_4^{2-} + \,^{·}OH \rightarrow SO_4^{·-} + OH^- \tag{3}$$

The ability of SO$_4^{2-}$ not only enhances charge separation but also generates SO$_4^{·-}$ as a strong oxidizing agent, accelerating the photocatalytic reaction.

The direct bandgap energy of semiconductors can be evaluated by Kubelka–Munk function. In addition, the energy band alignment can help to rationalize charge separation process and gain insights into the photocatalytic mechanism [40]. The detailed charge transfer process is proposed and illustrated in Fig. 7b. As the appearance of impurity energy level, ASZ photocatalysts can produce photogenerated electrons (e$^-$) and holes (h$^+$) under UV–vis light irradiation. The excited electrons can be successfully transferred from ZnO to Ag$^+$, and then Ag$^+$ is reduced to Ag NPs on the surface of ZnO nanoflakes. It is reported that the work function of ZnO (5.2 eV) exceeds that of Ag (4.3 eV), demonstrating that electrons migration from Ag to ZnO can proceed in order to attain a new Fermi level equilibration. Then the photo-generated electrons can be successfully transferred to Ag nanoparticles under the UV–vis light irradiation because conduction band level of ZnO is higher than the new Fermi energy. Thus photoinduced holes are located on the valence band (VB) of ZnO [23, 41]. Continual charge transfer can greatly inhibit the recombination of photoexcited electron–hole pairs and effectively separate charges. Thus, the produced e$^-$ migrate toward the oxygen molecules in water and generate superoxide radical anion O$_2^-$, further producing hydroxyl radical ·OH. Meanwhile, the produced h$^+$ transfer to the ZnO surface and react with the superficial H$_2$O molecules, −OH or SO$_4^{2-}$ groups, forming highly reactive ·OH and SO$_4^{·-}$. Moreover, the resulting ·OH may also react with

SO$_4^{2-}$ to produce SO$_4^{·-}$. Therefore, the reactive species as strong oxidants are applied in the decomposition of azo dyes and the improvement of photocatalytic performance.

4 Conclusions

In summary, novel nano-sized Ag$_2$SO$_4$/ZnO semiconductor composites were successfully synthesized by a facile solvothermal method. It reveals that Ag$_2$SO$_4$ nanoparticles are uniformly dispersed on ZnO nanoflakes surface. The optimized composition is investigated by executing photocatalytic experiment over different catalysts, which shows that 3ASZ possesses the highest photocatalytic performance towards RhB degradation under UV–vis light irradiation. Moreover, the photocatalytic efficiency of 3ASZ is superior to that of neat ZnO, Ag$_2$SO$_4$ particles and commercial TiO$_2$ (P25). The dramatically enhanced photocatalytic activity of Ag$_2$SO$_4$/ZnO composite is ascribed to the synergetic effect between photo-reduced Ag NPs and SO$_4^{2-}$ anchored on the ZnO surface, which effectively separate photogeneration electron–hole pairs. Therefore, the coupled semiconductors can be used as an effective strategy for photocatalysts development and provide potential applications in wastewater purification and environmental protection.

References

1. Tong H, Ouyang SH, Bi YP, Umezawa N, Oshikiri M, Ye GH (2012) Adv Mater 24:229
2. Boppana VBR, Jiao F (2011) Chem Commun 47:8973
3. Liu ZW, Pavaskar P, Aykol M, Cronin SB (2011) Nano Lett 11:1111
4. Zhang OF, Chou TP, Russo B, Jenekhe SA, Cao GZ (2008) Angew Chem Int Ed 47:2402
5. Miao G, Chen LF, Qi ZW (2012) Eur J Inorg Chem 35:5864
6. Mclaren A, Solis TV, Li GQ, Tsang SC (2009) J Am Chem Soc 131:12540
7. Tian CG, Zhang Q, Wu AP, Jiang MJ, Liang ZL, Jiang BJ, Fu HG (2012) Chem Commun 48:2858
8. Bai XJ, Wang L, Zong RL, Lv YH, Sun YQ, Zhu YF (2013) Langmuir 29:3097
9. Bloh JZ, Dillert R, Bohnemann DW (2013) ChemCatChem 5:774
10. Uddin MT, Nicolas Y, Olivier C, Toupance T, Servant L, Müller MM, Kleebe HJ, Ziegler J, Jaegermann W (2012) Inorg Chem 51:7764
11. Yoo DH, Cuong TV, Luan VH, Khoa NT, Kim EJ, Hur SH, Hahn SH (2012) J Phys Chem C 116:7180

12. Pelaez M, Falaras P, Likodimos V, Knontos AG, de la Cruz AA, O'shea K, Dionysiou DD (2010) Appl Catal B 99:378
13. Kong L, Jiang Z, Xiao TC, Jones MO, Edwards PP (2011) Chem Commun 47:5512
14. Zou CW, Rao YF, Alyamani A, Chu W, Chen MJ, Patterson DA, Emanuelsson EAC, Gao W (2010) Langmuir 26:11615
15. Wetchakun N, Chaiwichain S, Inceesungvorn B, Pingmuang K, Phanichphan S, Minett AI, Chen J (2012) Appl Mater Interfaces 4:3718
16. Li YZ, Zhang H, Guo ZM, Han JJ, Zhao XJ, Zhao QN, Kim SJ (2008) Langmuir 24:8351
17. Ye LQ, Liu JY, Gong CQ, Tian LH, Peng TY, Zan L (2012) ACS Catal 2:1677
18. Cheng HF, Huang BB, Wang P, Wang ZY, Lou ZZ, Wang JP, Qin XY, Zhang XY, Dai Y (2011) Chem Commun 47:7054
19. Zhang LL, Zhang HC, Huang H, Liu Y, Kang ZH (2012) New J Chem 36:1541
20. Liu Y, Hu JC, Ngo C, Prikhodko S, Kodambaka S, Li JL, Richards R (2011) Appl Catal B 106:212
21. Chen L, Hu J, Richards R (2008) ChemPhysChem 9:1069
22. Cao TP, Li YJ, Wang CH, Shao CL, Liu YC (2011) Langmuir 27:2946
23. Lu WW, Gao SY, Wang JJ (2008) J Phys Chem C 112:16792
24. Niu YX, Xing MY, Tian BZ, Zhang JL (2012) Appl Catal B 115–116:253
25. Pang ML, Hu JY, Zeng HC (2010) J Am Chem Soc 132:10771
26. Subash B, Krishnakumar B, Pandiyan V, Swaminathan M, Shanthi M (2012) Sep Purif Technol 96:204
27. Zhang YW, Tian JQ, Li HY, Wang L, Qin XY, Asiri AM, Al-Youbi AO, Sun XP (2012) Langmuir 28:12893
28. Virkutyte J, Varma RS (2012) RSC Adv 2:2399
29. Butler MA (1977) J Appl Phys 113:7371
30. Tanaka A, Sakaguchi S, Hashimoto K, Kominami H (2013) ACS Catal 3:79
31. Chen DL, Li T, Chen QQ, Gao JB, Fan BB, Li J, Li XJ, Zhang R, Sun J, Gao L (2012) Nanoscale 4:5431
32. Iliev V, Tomova D, Bilyarska L, Tyuliev G (2007) J Mol Catal A 263:32
33. Burch R, Breen JP, Meunier FC (2002) Appl Catal B 39:283
34. Chen WT, Hsu YJ (2010) Langmuir 26:5918
35. Kansal SK, Singh M, Sud D (2007) J Hazard Mater 141:581
36. Zhang L, He YM, Ye P, Wu Y, Wu TH (2013) J Alloy Compd 549:105
37. Naik B, Parida KM, Gopinath CS (2010) J Phys Chem C 114:19473
38. Gaya UI, Abdullah AH, Zainal Z, Hussein MZ (2009) J Hazard Mater 168:57
39. Wang C, Zhao JC, Wang XM, Mai BX, Sheng GY, Peng PA, Fu JM (2002) Appl Catal B 39:269
40. Uddin MT, Nicolas Y, Olivier C, Toupance T, Müller MM, Kleebe HJ, Rachut K, Ziegler J, Klein A, Jaegermann W (2013) J Phys Chem C 117:22098
41. Zheng YH, Zheng LR, Zhan YY, Lin XY, Zheng Q, Wei KM (2007) Inorg Chem 46:6980